

Article

The Effect of Village Morphological Variation Caused by Economic Development on Residents' Health and Rural Ventilation in Tianjin

Fusuo Xu ¹, Zhi Gao ^{2,1,*} , Yuchen Xing ¹, Zihao Wu ¹, Jianshun Zhang ³, Yimin Liao ¹ and Yongyu Hu ¹¹ School of Architecture and Urban Planning, Nanjing University, 22 Hankou Road, Nanjing 210093, China² Joint International Research Laboratory of Eco-Urban Design, Tongji University, Ministry of Education, 1239 Siping Road, Shanghai 200092, China³ Department of Mechanical and Aerospace Engineering, Syracuse University, Syracuse, NY 13210, USA

* Correspondence: zhgao@nju.edu.cn; Tel.: +86-025-8359-7332

Abstract: Many multi-story residential buildings have been built in villages to improve the living quality of rural residents in China. Therefore, village morphology has dramatically changed compared to the past. Since northern China continues to suffer from environmental problems, improving village ventilation by optimizing village morphology is essential for creating a good rural environment. In this study, 17 morphology models were categorized based on 383 actual villages in Tianjin. In addition, the ventilation capacity of courtyards and streets and residents' health risks of different morphology cases were analyzed. For the northwest wind direction, the ventilation capacity of the courtyards in the northern part of the village can be improved when there are multi-story residences in the north or west of the village. Accordingly, in the southeast wind direction, multi-story buildings in the south or east of the village can improve the courtyard ventilation in the southern part of the village. In addition, multi-story buildings in the west or east of the village can form ventilation corridors in the northwest or southeast wind direction. The morphologies without multi-story buildings in the west or east of the village were recommended to be applied in the village planning in Tianjin due to good ventilation capacity and low exposure risks.

Keywords: village morphology; ventilation capacity; health risk; CFD simulations**Citation:** Xu, F.; Gao, Z.; Xing, Y.; Wu, Z.; Zhang, J.; Liao, Y.; Hu, Y.

The Effect of Village Morphological Variation Caused by Economic Development on Residents' Health and Rural Ventilation in Tianjin.

Buildings **2022**, *12*, 1393. <https://doi.org/10.3390/buildings12091393>

Academic Editor: Theodore Stathopoulos

Received: 8 August 2022

Accepted: 31 August 2022

Published: 6 September 2022

Publisher's Note: MDPI stays neutral with regard to jurisdictional claims in published maps and institutional affiliations.**Copyright:** © 2022 by the authors. Licensee MDPI, Basel, Switzerland. This article is an open access article distributed under the terms and conditions of the Creative Commons Attribution (CC BY) license (<https://creativecommons.org/licenses/by/4.0/>).

1. Introduction

As China's economy continues to grow, the scale and morphology of cities have changed dramatically compared to the past. The city characteristics of the high building and population density reduce urban ventilation capacity [1,2], accumulate pollutants [3,4], and increase urban heat island intensity [5,6]. At the same time, the construction of Chinese villages has been developing rapidly since 2000. Many multi-story and high-rise residential buildings were built to improve the living environment and quality of rural people. As a result, the village morphology has changed dramatically. However, the study of the influence of village morphology on ventilation and residents' health is still very lacking and unclear. The environmental and health problems caused by rural development need to be studied to provide suggestions for subsequent rural planning.

Northern China suffers from the problem of haze in winter [7]. In addition to vehicle exhaust and industrial emissions in cities, winter heating and traditional cooking in the countryside are also major contributors to haze [8,9]. The emissions of NO_x, NMVOCs, SO₂, and PM_{2.5} from rural household heating in Beijing were 11.5 kt, 29.3 kt, 43.1 kt, and 34.7 kt, respectively, while those for household cooking totaled 1.55 kt, 4.02 kt, 6.55 kt, and 3.99 kt [10]. In the Beijing-Tianjin-Hebei region of China, the highest PM_{2.5} concentrations have been observed [11]. With the implementation of environmental management policies, such as coal-to-gas and coal-to-electricity, air quality and other environmental problems in

rural areas in northern China have improved somewhat [12]. Exploring the optimal village morphology and rural planning scheme to improve rural ventilation is an effective way to build a green countryside and livable environment.

In recent years, the influence of morphology on urban wind and thermal environments has become a research hotspot [13–19]. The correlation analysis between morphological indices and the wind and thermal environment using ideal or real neighborhood models can help architects and planners to develop sustainable urban development schemes that facilitate urban ventilation and mitigate urban heat island intensity. The study of rural morphologies is more scarce than urban ones. Research on the rural environment is urgently needed due to the large number of people living in rural areas in China. Previous studies on the influence of building geometry (roof shape, arcade, lift-up design) [20–26], morphological parameters (building density, aspect ratio, building coverage ratio, etc.) [27–35] on urban ventilation do not apply to the countryside, as the shape and scale of the rural house in northern China are strictly regulated. Therefore, the Chinese countryside morphology needs specialized study.

Computational fluid dynamics (CFD), geographic information systems (GIS), and weather research and forecasting models (WRF) have become the primary methods for the study of urban ventilation [36–41]. GIS is suitable for urban scale studies, which require dividing the city into 100–500 m resolution grids and calculating morphological indices and correlation for each grid [42,43]. WRF is applicable to larger-scale regional climate and atmospheric studies. CFD is more suitable for the analysis of rural problems. The size of the Chinese countryside is usually less than 1 km², so the computational cost of the countryside model is usually appropriate for using CFD. In addition, the CFD method can easily obtain wind fields and calculate the ventilation index to facilitate a comparison of different design and planning solutions.

In short, current research has focused on urban morphology and environmental issues, and very little attention has been paid to the morphology changing of the Chinese countryside. However, with a large proportion of the population in rural China [44], there is a need to focus on rural people's health and environmental issues. In addition, the impact of countryside morphology variation caused by many new multi-story and high-rise buildings on the village ventilation is still unclear, and there is a lack of research on this issue. Therefore, this study categorized the real village morphology in Tianjin into 17 morphology types and analyzed the ventilation capacity and residents' health risk using the CFD method to guide the sustainable development of Chinese villages.

2. Morphological Analysis

2.1. Study Region

Tianjin is the core city of the economic circle of China's capital and the second largest city in northern China, with a population of 13.73 million and an area of 11,966.45 km². The traditional North China village consists of hundreds of single-story courtyard houses arranged in regular rows. Conversely, residential areas in urban areas tend to be multi-story and high-rise residential buildings. With the rapid development of China's economy, the village morphology has changed dramatically compared to the last century. In addition to the overall demolition of villages, a large number of villages have built multi-story buildings outside the original village boundaries. New high-rise and multi-story buildings significantly impact the ventilation and pollutant dispersion in the village. Tianjin has 16 administrative districts. The areas that adopted the development policy of preserving traditional rural buildings (one story) and building high-rise and multi-story buildings around villages are mainly in Jinghai, Jizhou, Baodi, and Wuqing districts. These districts are far from the city center. Because of its proximity to Hebei Province and its cultural integration with the Hebei region, the Jinghai district represents the general state of rural development in the Beijing-Tianjin-Hebei region, as shown in Figure 1A.

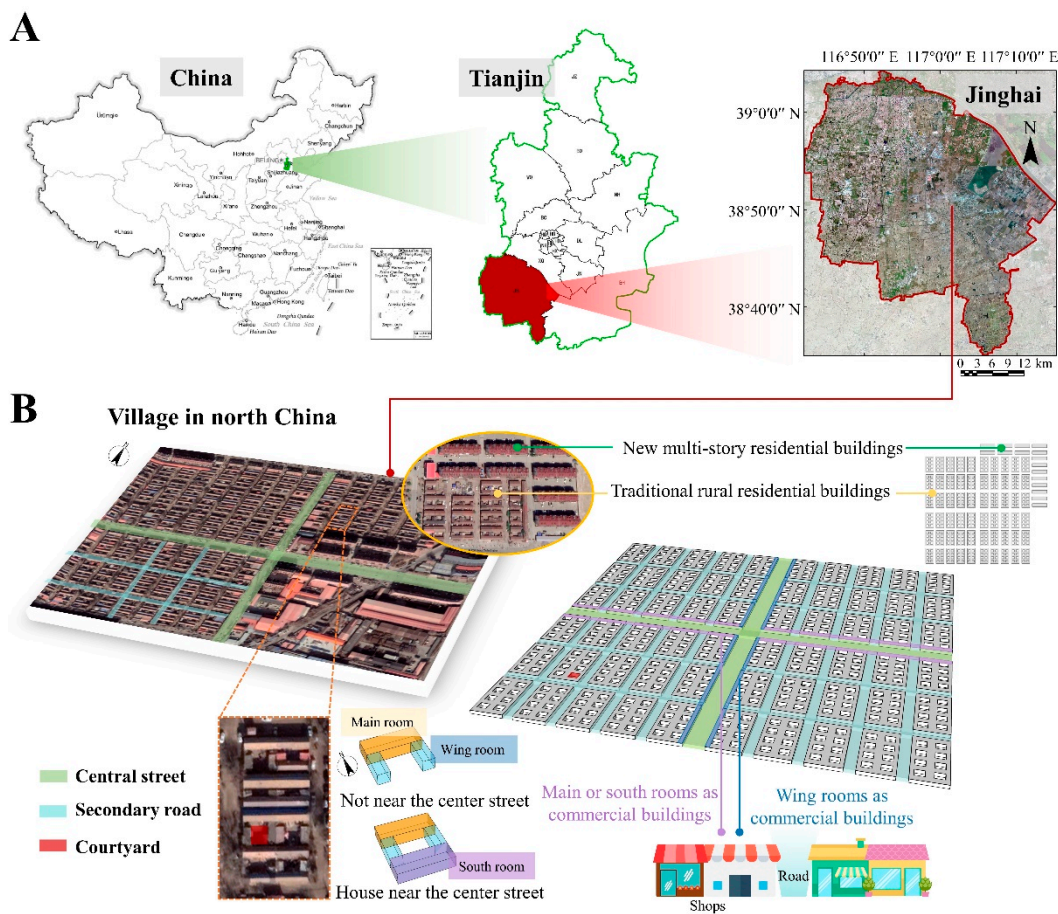


Figure 1. Overview of Tianjin village. (A) Study area. (B) Architectural and living space information in the village.

Jinghai has 383 administrative villages with a resident population of 818,000. Compared with 20 years ago, the village morphology of Jinghai has changed considerably. Traditional rural architecture in northern China evolved based on Chinese courtyard houses. Each house consists of the main and wing rooms, as shown in Figure 1B. The main room faces south with the back to the north. The houses on the west-east street usually also have south rooms. Each village usually has one or two central streets for commercial and recreational activities. Therefore, the rooms on both sides of the central street are generally shops.

2.2. Morphological Statistics

This study investigated and analyzed the morphology and scale of 383 villages in Jinghai. As shown in Figure 2, the length and width of villages are mainly concentrated in 400–600 m, accounting for 34.5% and 37.2%, respectively. The highest percentage of the village area is 200,000–300,000 m² with 27.2%. In addition, the village perimeter is concentrated in the range of 1500–2000 m. An idealized village model of 432 × 420 m² was established based on village-scale statistics. Four village morphology types were extracted from the real villages, as shown in Figure 3. “LL” morphology, which is similar to “L” morphology, was also investigated in this study. Overall, five morphology types were used in this study, namely “I”, “L”, “LL”, “C”, and “O”, as shown in Figure 4. In North China, the building dimensions of the village area are strictly restricted by planning codes (village houses have almost the same dimensions), resulting in a neat and uniform rural texture. Therefore, using an idealized model is appropriate for this study.

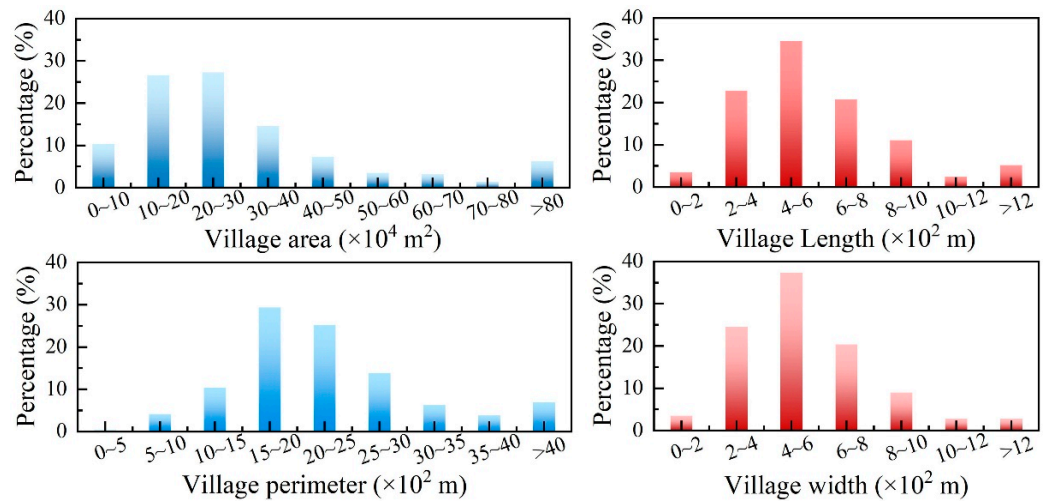


Figure 2. Village scale in Jinghai district of Tianjin.

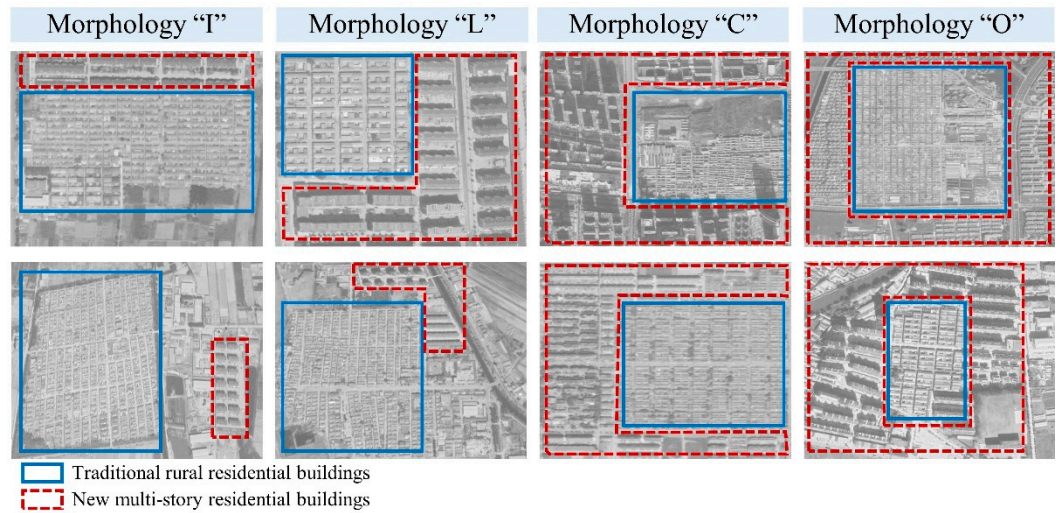


Figure 3. Analysis of real village morphology.

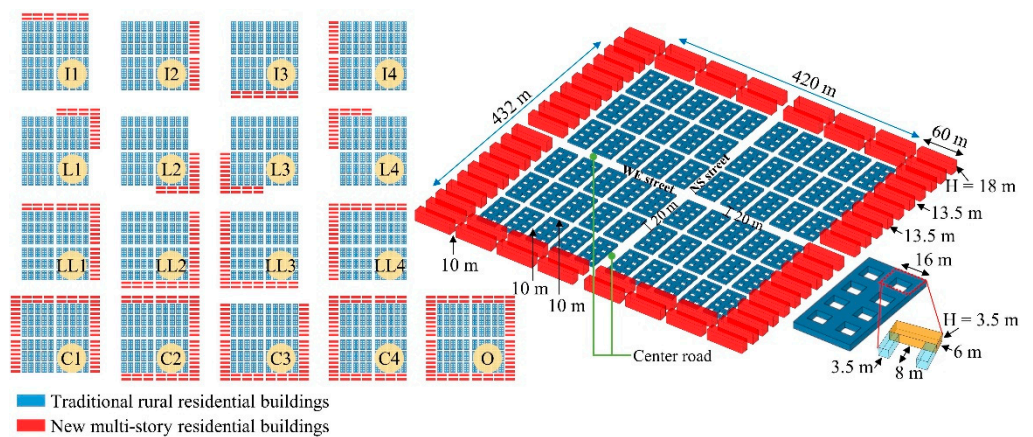


Figure 4. The idealized village morphology model used in this study.

The dimensions of traditional rural buildings and new multi-story buildings are shown in Figure 4. The dimensions of a new multi-story building are $L \times W \times H = 60 \text{ m} \times 13.5 \text{ m} \times 18 \text{ m}$. The new multi-story buildings represent typical 6-story residential buildings in the village of northern China. In addition, the height of traditional residential buildings is 3.5 m. In the

village, the two central streets are 20 m wide, and the other streets are 10 m wide. A total of 17 morphology models (five types) were used to analyze the effects of different morphologies on rural ventilation and the residents' health.

3. Methodology

3.1. CFD Simulation Method

Different village morphologies have different effects on rural ventilation and residents' health. Therefore, it is essential to obtain the optimal typical village morphology for rural development by comparing different morphology cases. A total of 34 CFD simulation cases (17 morphological models \times two typical wind directions) were set up in this study. In Tianjin, southeast winds prevail in summer, and northwest winds prevail in winter. The monthly average wind speed is 2.3–3.6 m/s annually [45]. Therefore, the wind speed of this study was set at 3 m/s for both northwest and southeast wind directions. The velocity-inlet profile was defined using Equation (1):

$$U_Z = \frac{U_{ABL}^*}{k} \ln\left(\frac{z + z_0}{z_0}\right) \quad (1)$$

where U_Z is the wind speed (m/s) at the height of z (m). z_0 is the roughness length, z_0 was set as 0.03, representing the roughness of farmland. k is the von Karman constant (0.41) [46]. The friction velocity of the atmospheric boundary layer (U_{ABL}^*) can be calculated by Equation (2):

$$U_{ABL}^* = \frac{kU_r}{\ln\left(\frac{z_r + z_0}{z_0}\right)} \quad (2)$$

where U_r is the reference velocity (m/s) at the reference height z_r (m). The wind velocity was set as 3 m/s at the reference height of 10 m, according to the meteorological data of Tianjin. Turbulent kinetic energy (k_z , m^2/s^2) and turbulent dissipation rate (ε_z , m^2/s^3) were calculated by Equations (3) and (4):

$$k_z = \frac{U_{ABL}^{*2}}{\sqrt{C_\mu}} \quad (3)$$

$$\varepsilon_z = \frac{U_{ABL}^{*3}}{k(z + z_0)} \quad (4)$$

where C_μ is a constant (0.09).

The Reynolds-averaged Navier–Stokes (RANS) equations with a realizable k - ε turbulence model were used to solve the turbulent wind flow. The standard wall function was used to solve the flow close to walls. In addition, the Semi-Implicit Method for Pressure-Linked Equations (SIMPLE) algorithm was used for the pressure-velocity coupling of the transport equations. The species transport model was used to simulate the inert gas pollutant dispersion. The second-order schemes were applied to discretize the convection and diffusion terms. This study assumes convergence criteria for all variables' residuals $<10^{-4}$ and a fluctuation range of $<5\%$ for parameter values of multiple monitoring sites.

The boundary conditions and computational domains were set, as shown in Table 1 and Figure 5A. The boundary of the calculation domain is 10H away from the building complex (H is the highest building height), and the blockage rate is $<3\%$ according to AII guidelines [47]. This study set up two inlets and two outlets to establish northwest and southeast wind direction. The symmetry condition was used for the top boundary of the computational domain. Building surfaces and ground were modeled using the no-slip wall type.

Table 1. Boundary condition setting in this study.

Location	Type	Profiles/Conditions
Inlet	Velocity inlet	Equations (1), (3) and (4), 3 m/s
Outlet	Outflow	$\frac{\partial}{\partial x}$ and $\frac{\partial}{\partial y}(u, v, w, k, \epsilon) = 0$
Top	Symmetry	$\frac{\partial}{\partial z}(u, v, w, k, \epsilon) = 0$
Ground	Wall	No-slip
Building	Wall	No-slip

Note: two inlet and outlet boundaries for each simulation case.

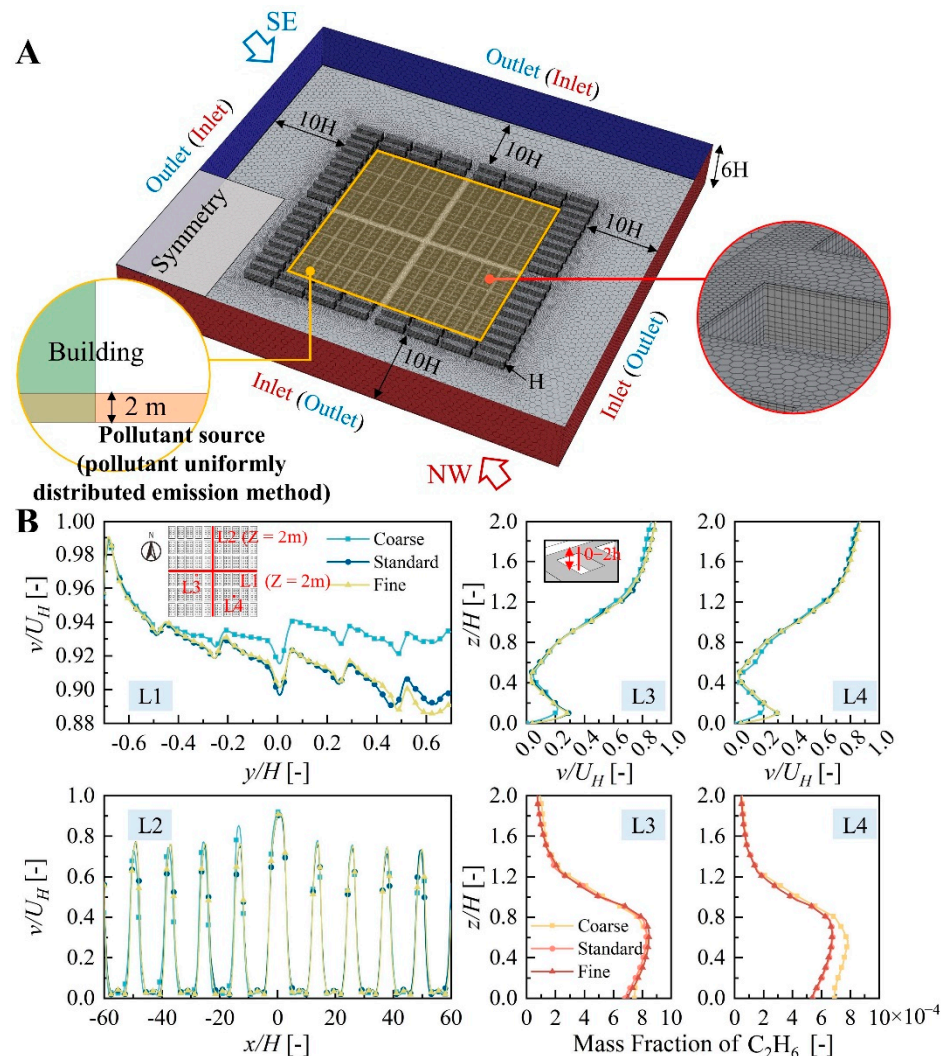


Figure 5. Computational domain and grid sensitivity analysis. (A) Computational domain dimensions and boundary condition settings. (B) Grid sensitivity verification.

3.2. Grid Sensitivity and Validation

ANSYS Fluent Meshing was used to generate the mesh. The grid becomes progressively sparser from the building complex to the edge of the computational domain through the Body of Influence (BOI) control to achieve a reasonable grid number. BOI1 was set to $X \times Y \times Z = 600 \times 573 \times 20 \text{ m}^3$, and BOI2 was set to $660 \times 633 \times 26 \text{ m}^3$, and they extended 20 m and 30 m at the outer edge (XY plane) of the multi-story buildings (morphology O), respectively. This study created more than five layer grids under pedestrian height level ($Z = 1.5 \text{ m}$) and ensured the $y+$ value is less than 300 for the wall-type boundaries. Three grids were used to investigate the grid sensitivity, and their dimensions in the study area were 1.5 m, 3 m, and 6 m, respectively. The coarse, standard, and fine grids are 4.14 million,

7.09 million, and 9.04 million, respectively. As shown in Figure 5B, the wind speed ratios and mass fractions of C_2H_6 for standard and fine grids in the two horizontal and two vertical reference lines can match well. In contrast, the wind speed ratio of the coarse grid is very different from the other two grids at the L1 location. For the mass fraction of C_2H_6 , the coarse grid still does not match the other two grids well at the L4 location, with a maximum difference of 29.5%. Therefore, the standard grid can predict the outdoor flow field accurately.

Although wind tunnel test data for the same experimental model as this study are not available, previous experimental studies have provided wind speed and pollutant data from wind tunnel experiments for the building complex [48,49]. These experimental data can be used to verify the accuracy of the CFD simulation method used in this study. The authors used the same turbulence model, boundary conditions, grid size distribution, and other setup methods as this study verified with these experimental wind speed and pollutant data in the authors' previous paper [50–52]. In particular, for the validation of wind speed, the difference at the highest point of wind speed was only 11.7%, which is less than the 15% recommended by the Architectural Institute of Japan. In addition, several statistical metrics were used to quantify the accuracy of the pollutant simulations, including normalized mean square error, fractional bias, and correlation coefficient. These statistical metrics met the criterion recommended by Santiago et al. [53]. Therefore, the CFD simulation setup used in this study is accurate.

3.3. Analysis Indices

3.3.1. Normalized Pollutant Concentration

In order to evaluate the pollutant dispersion and ventilation capacity in different village morphologies, several analysis indices were applied in this study. The normalized pollutant concentration (C^*) was applied to evaluate pollutant dispersion in different simulation cases.

$$C^* = \frac{C \times U_r \times H_r^2}{\dot{m} \times V_e} \quad (5)$$

where C is the pollutant concentration (kg/m^3). The pollutant uniformly distributed emission method [54] was used to study the pollutant dispersion and ventilation capacity with an emission rate (\dot{m}) of $10^{-5} kg/(m^3 \cdot s)$ (C_2H_6 was assumed). In addition, V_e is the volume of emission zone, which is the 0–2 m zone in the village in this study.

3.3.2. Purging Flow Rate

To quantify the ventilation capacity of different zones, purging flow rate (PFR, m^3/s) was used to analyze the ventilation capacity of the courtyard and street spaces in different village morphologies. It is worth noting that PFR can only be used to compare the ventilation capacity of the same volume space, such as the courtyard of this study. In addition, the two central streets were divided into 41 zones with the same volume ($20 \times 20 \times 3.5 m^3$) to evaluate the ventilation capacity of the different street zones.

$$PFR = \frac{\dot{m} \times V_{tar}}{\bar{C}} \quad (6)$$

where V_{tar} is the volume (m^3) of the target zones, such as zone S21 in Figure 6. \bar{C} is the average pollutant concentration (kg/m^3) of the target zone. The numbered naming of the courtyard and street spaces is shown in Figure 6.

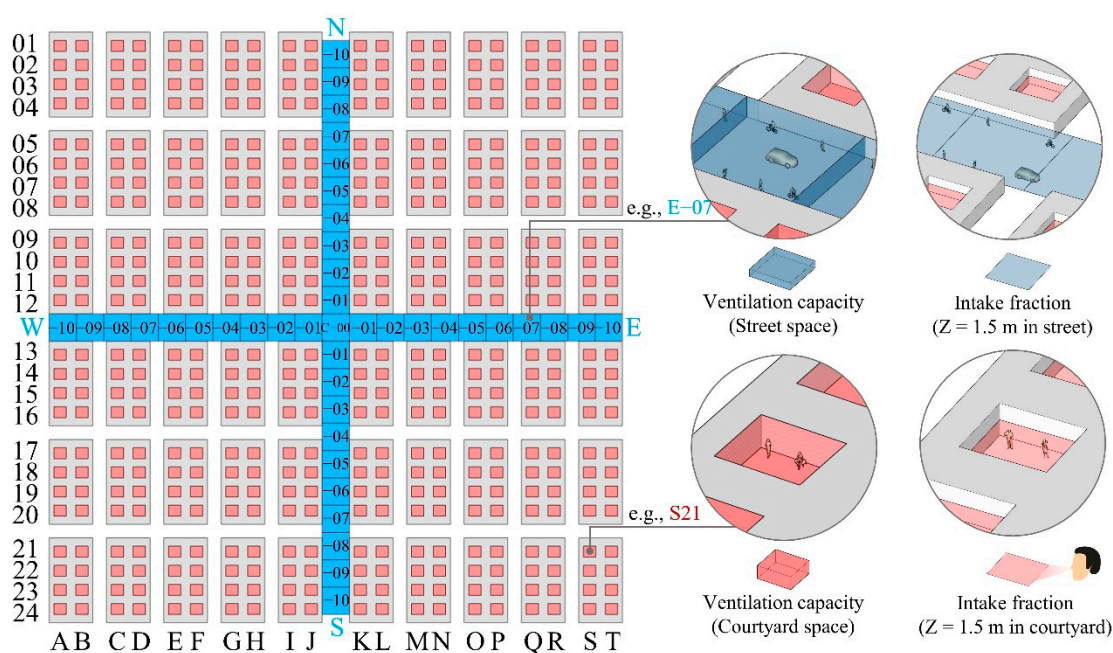


Figure 6. Schematic of the space naming and analysis index calculation zone.

3.3.3. Intake Fraction

The average values of pollutant concentration at 1.5 m in the courtyard and street spaces were calculated to evaluate the health risk of residents, as shown in Figure 6. The individual intake fraction (IF) was calculated using Equation (7) [55].

$$IF = \frac{\bar{C} \cdot BR_i \cdot T_i}{E} \quad (7)$$

where BR_i is the breathing rate, $2.85 \text{ m}^3/\text{h}$ [56]. T_i is the time spent on some activities (h), and one hour was assumed in this study. E is the pollutant emissions from the study area ($m \times \text{emission volume} \times \text{one hour, kg}$).

4. Results and Discussion

4.1. Pollutant Field

It can be seen from Figure 7A that pollutants tend to accumulate in the courtyard, and the pollution level of the different courtyards was analyzed by the ventilation capacity index (Section 4.2). Therefore, this section only exhibited the pollutant contours of the central street used for shopping and activities. As shown in Figure 7B, the southern part of the NS street is more likely to accumulate pollutants under the northwest wind direction. Morphology I3, L3, LL2, and C2 showed high pollutant concentration zones in the southernmost street. In addition, L4, LL3, and C3 exhibited high pollutant concentration zones in the central part of NS street. For WE street (Figure 7C), the pollutant concentration of morphology I1, LL1, LL4, C2, and C4 in the eastern part of the street is significantly lower than the other morphologies. Moreover, morphology L4, C1, and O accumulated higher pollutant concentrations only in the easternmost part. The areas of high pollutant concentrations in I2-I4, L1-L3, LL2, LL3, and C3 are significantly more than in the other morphologies. For the overall assessment of NS and WE streets in the northwest wind direction, morphology I1, LL1, LL4, and C4 are beneficial for street ventilation, followed by morphology L4, C1, and O.

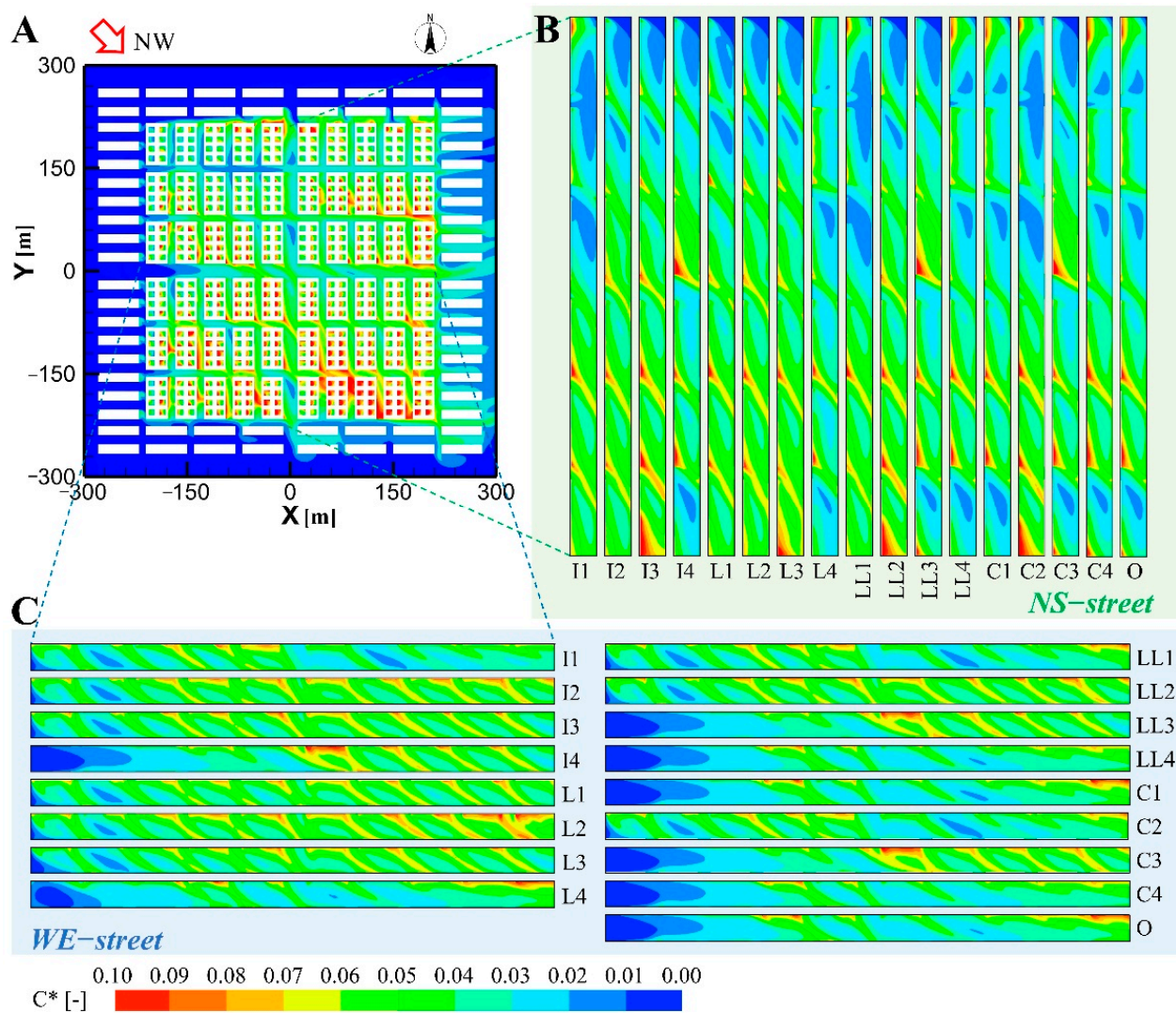


Figure 7. Contours of normalized pollutant concentration (C^*) at the pedestrian level ($Z = 1.5$ m) for northwest wind direction. (A) Morphology O. (B) NS street of different morphology. (C) WE street of different morphology.

As shown in Figure 8A, pollutant concentrations are higher in the northwestern part of the village in the southeast wind direction. The air quality of residential houses downwind is usually worse. For NS streets (Figure 8B), morphology I1, L1, LL4, and C4 exhibited areas of high pollutant concentrations in the northern part of the street. In addition, morphology I2, LL1, LL4, and C1 have higher pollutant concentrations in the middle of the street than the other morphologies. As shown in Figure 8C, the street pollutant concentration of LL4 is significantly higher for WE streets than the other morphologies. In addition, WE street space pollutant concentrations of morphology I3, LL2, LL3, and C2 are lower than other morphologies, followed by morphology L2, C3, C4, and O. In conclusion, for the southeast wind direction, the morphology I3, LL2, LL3, and C2 are more beneficial for street ventilation.

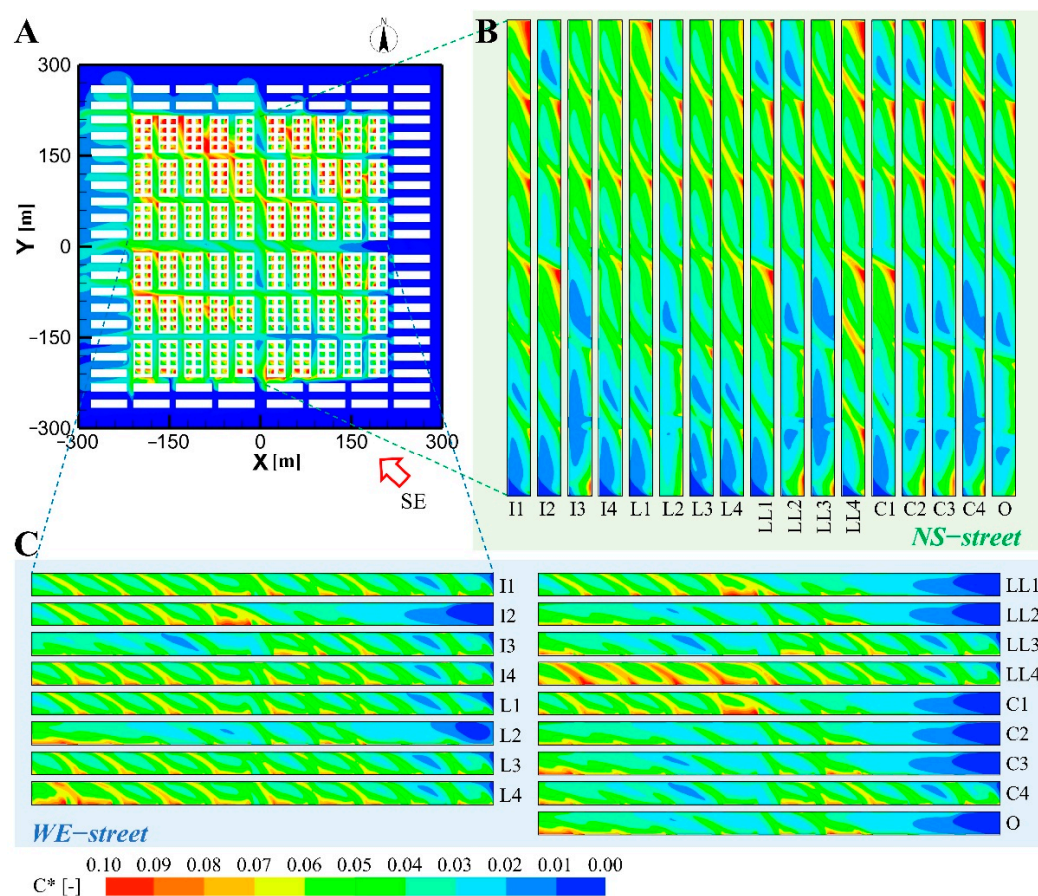


Figure 8. Contours of normalized pollutant concentration (C^*) at the pedestrian level ($Z = 1.5$ m) for southeast wind direction. (A) Morphology O. (B) NS street of different morphology. (C) WE street of different morphology.

4.2. Ventilation Capacity

4.2.1. Courtyard

The PFR values of the courtyards of different village morphologies in the northwest wind direction are shown in Figure 9. Residential houses on the windward side of the village edge can obtain better ventilation capacity and air quality. The different village morphologies affect the airflow into the village's interior and, thus, the residential courtyards' ventilation capacity. Morphology I1, L1, LL1, C1, and O exhibited high PFR values in the northern part of the village (zones I and II). These morphologies are present in the north of the village with multi-story buildings, bringing more incoming wind and increasing wind speed. The presence of new multi-story buildings in the north of the village for morphology C2 and in the west of the village west for morphology C4 also produces high ventilation areas in zone I. In addition, morphology L4 and LL4 also have multi-story buildings in the north or west of the village, and they all obtain high ventilation capacity areas in the northern part of the village. Morphology I4, LL3, and C3 all form two ventilation corridors, which help improve the courtyard's ventilation capacity on this path. Morphology L4, LL4, C1, C4, and O form not only high ventilation capacity areas but also ventilation corridors. In general, multi-story buildings in the west of the village are conducive to generating ventilation corridors.

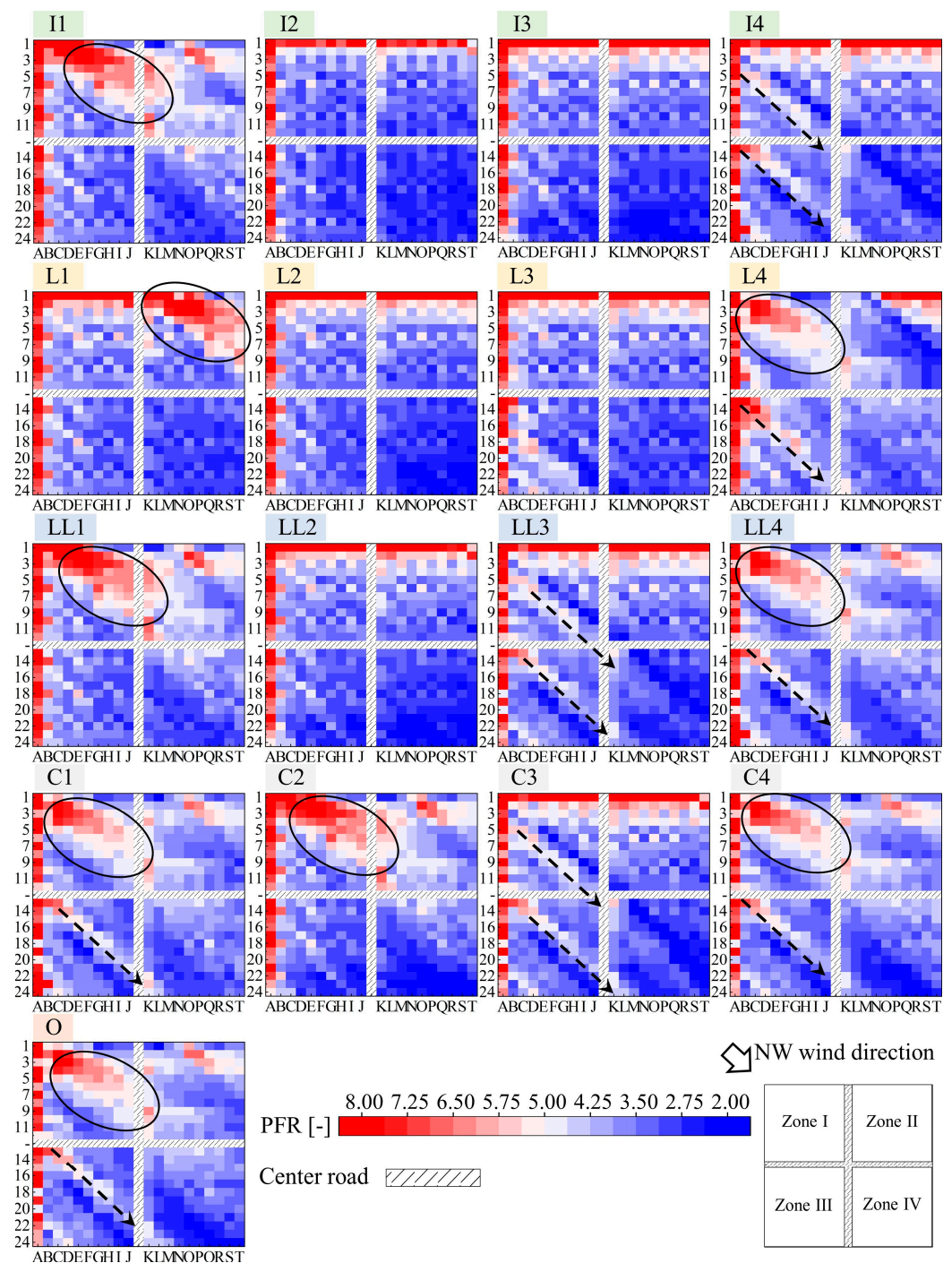


Figure 9. Analysis of the ventilation capacity of courtyards under northwest wind direction.

The ventilation capacity analysis of courtyards in the southeast wind direction is shown in Figure 10. For the presence of multi-story buildings in the village east, morphology L2, LL2, and C2, the southern part of their villages (zone IV), were formed high ventilation capacity zones. In addition, multi-story buildings in the south of the village, morphology I3, L3, LL3, and C3, and the southern part of their villages (zones III and IV) also formed high ventilation capacity zones. When multi-story buildings exist in the village east, it is easy to develop ventilation corridors to promote courtyard ventilation in one of the paths parallel to the wind direction. Morphology I2, LL1, and C1 all formed two ventilation corridors. Morphology L2, LL2, C2, C3, and O have not only high ventilation

capacity areas but also a ventilation corridor. Therefore, Morphology L2, LL2, C2, C3, and O are the preferable village development morphology in the southeast wind direction.

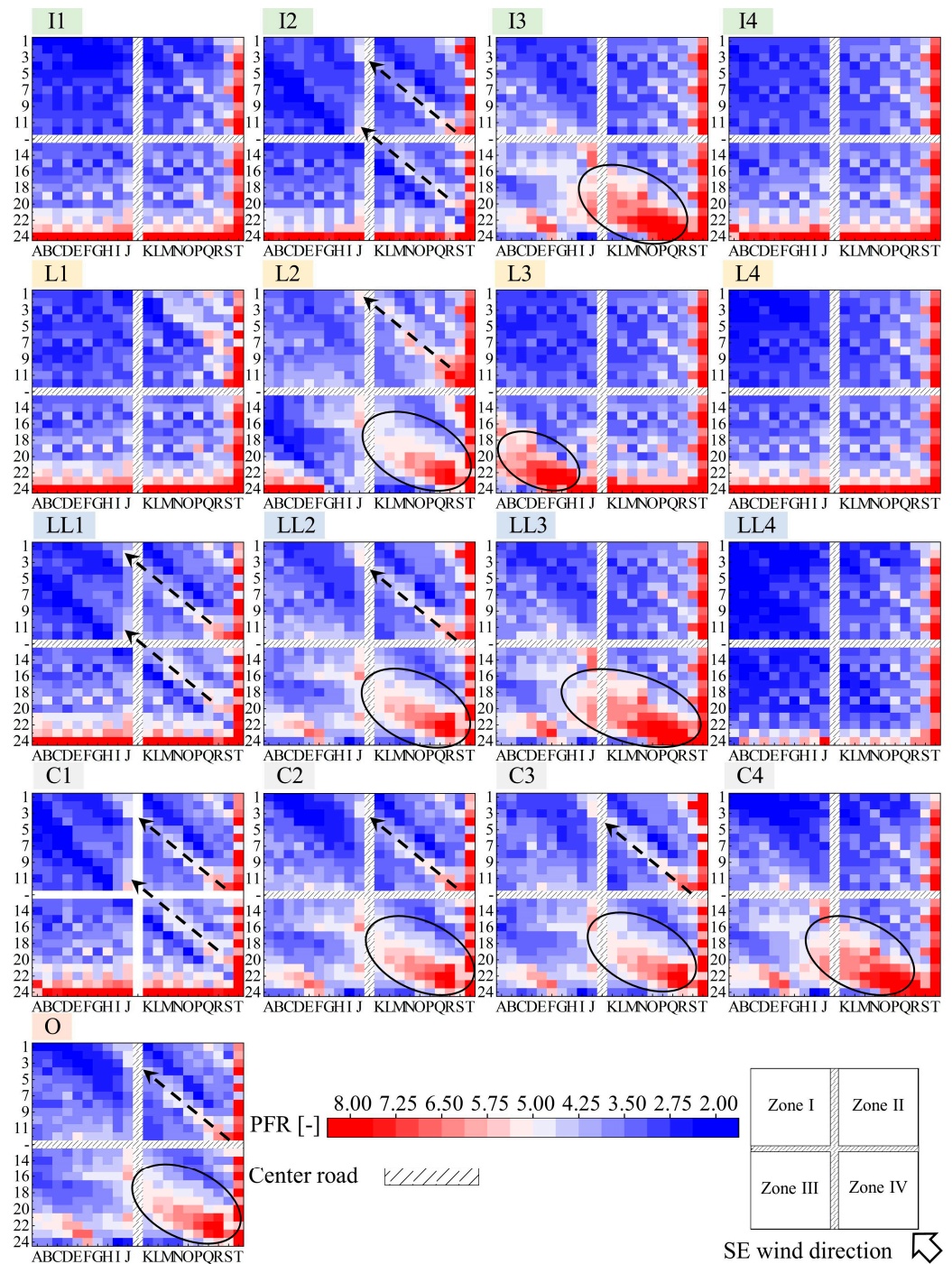


Figure 10. Analysis of the ventilation capacity of courtyards under southeast wind direction.

4.2.2. Street

The distribution of PRF values in street space is shown in Figure 11. In the northwest wind direction, there is more fresh air inflow in the northern part of NS street and the western part of WE street, so the PFR value is higher. However, the ventilation capacity of morphology L4 is poor in the northern part of the NS street. Furthermore, the high PFR zones of morphology LL4, C1, C4, and O are also less than other morphologies. They exhibited high PFR value zones in the southern part of the NS street, as shown in Figure 11A.

As shown in Figure 11B, morphology L1-L3, L1, L2, LL1, LL2, and C2 also have not high PFR zones in the western part of WE streets. These morphologies have a worse ventilation capacity for WE street in the northwest wind direction.

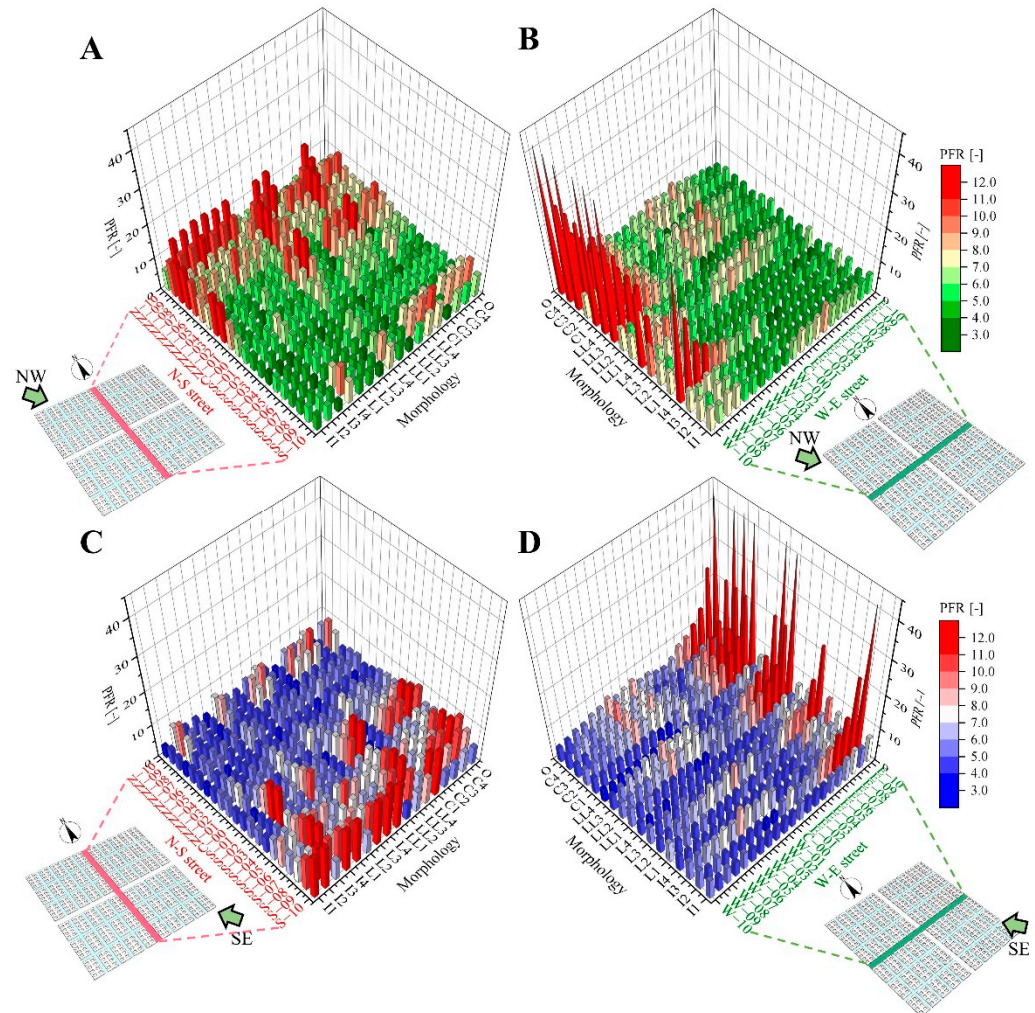


Figure 11. Ventilation capacity of the different zone in the central street. (A) and (B) under northwest wind direction (NW). (C) and (D) under southeast wind direction (SE).

For the southeast wind direction, the high ventilation capacity zone in the south of NS street is much less for morphology L2 and LL4. In addition, morphology I2, L2, LL1, LL2, C1–C3, and O also have one high PFR value zone in the northern part of the NS street, as shown in Figure 11C. For WE streets, the high PFR value zones of morphology I1, I3, I4, L3, L4, LL4, and C4 are much less. However, morphology I2, L2, LL1, LL2, C1–C3, and O have 3–4 high ventilation capacity zones with PFR values greater than 10, as shown in Figure 11D.

4.3. Health Risks

4.3.1. Courtyard

The IF value map of the courtyards in the northwest wind direction is shown in Figure 12. Some morphologies have high exposure risk areas, such as morphology I3, I4, L2, LL2, LL3, C2–C4, and O. All of these morphologies showed aggregation areas of exposure risk that were significantly higher than the average IF. However, the low IF areas of morphology I1, L4, LL1, LL4, and C1 are more predominant. The resident living in these village morphologies have a healthier environment. Zone IV of the village is more prone to

high exposure risk areas, especially when there are multi-story buildings in the southern part of the village.

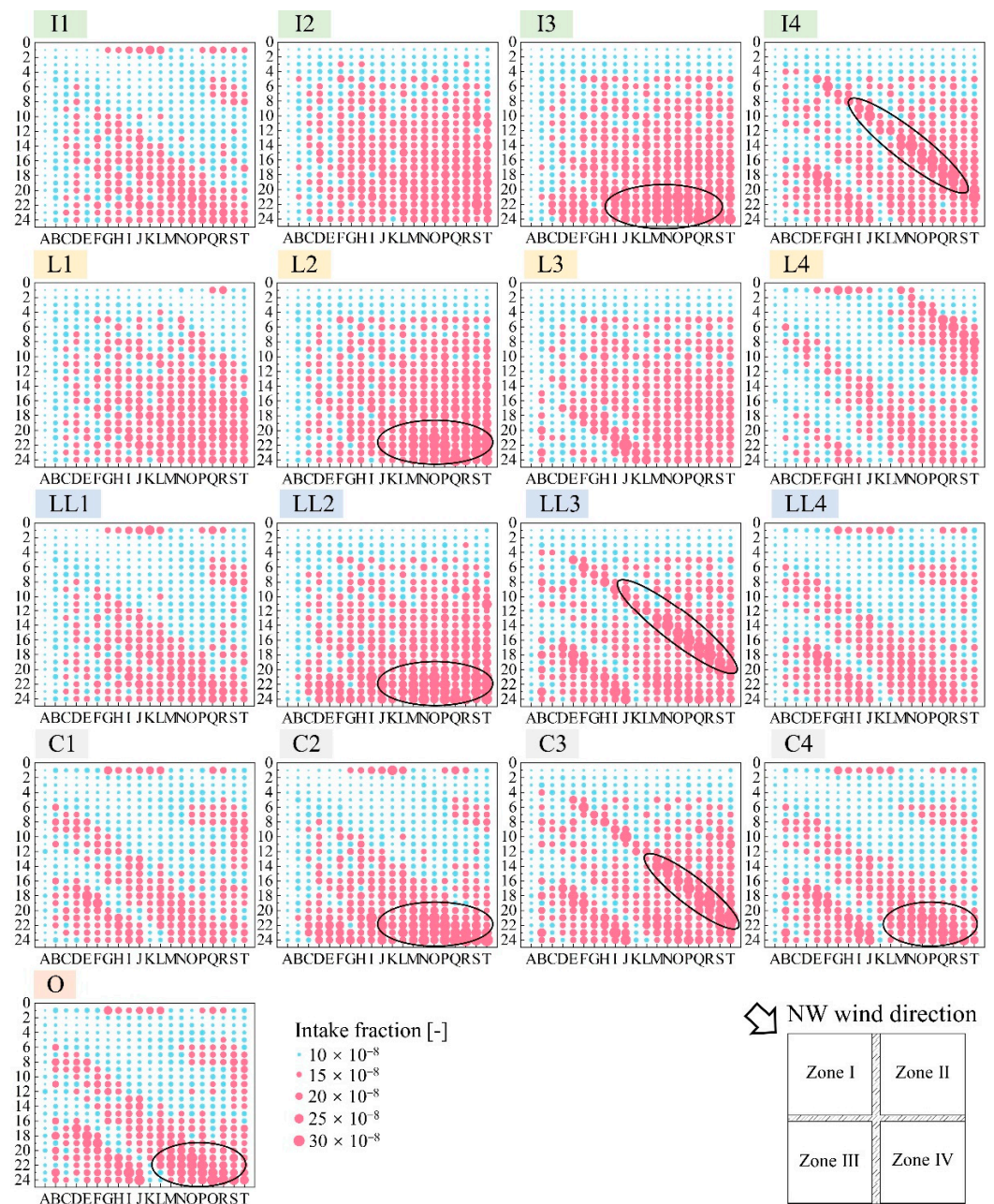


Figure 12. Analysis of the intake fraction of courtyards in the northwest wind direction. The red circles are intake fractions greater than 15×10^{-8} , and the blue circles are intake fractions less than 15×10^{-8} . 15×10^{-8} is the average value of intake fraction for all courtyards.

For the southeast wind direction, large areas of low exposure risk exist in the southern part of the village, as shown in Figure 13. Morphology I1, I2, L4, LL1, LL4, C1, C2, C4, and O all had high exposure risk areas in the northern part of the village that was significantly higher than the average IF. The accumulation of pollutants can dramatically threaten the residents' health in these areas. However, the low-exposure risk areas of morphology I3, L2, L3, LL2, LL3, and C3 are more predominant. Although large areas of low exposure risk exist in morphology C2, C4, and O, they also have high pollutant concentration accumulation areas. Therefore, the overall exposure risk evaluation of different morphologies still needs to be further analyzed by the average IF value and the

percentage of low-risk areas. In addition, for the southeast wind direction, high exposure risk areas are easily formed when there are multi-story buildings in the northern part of the village.

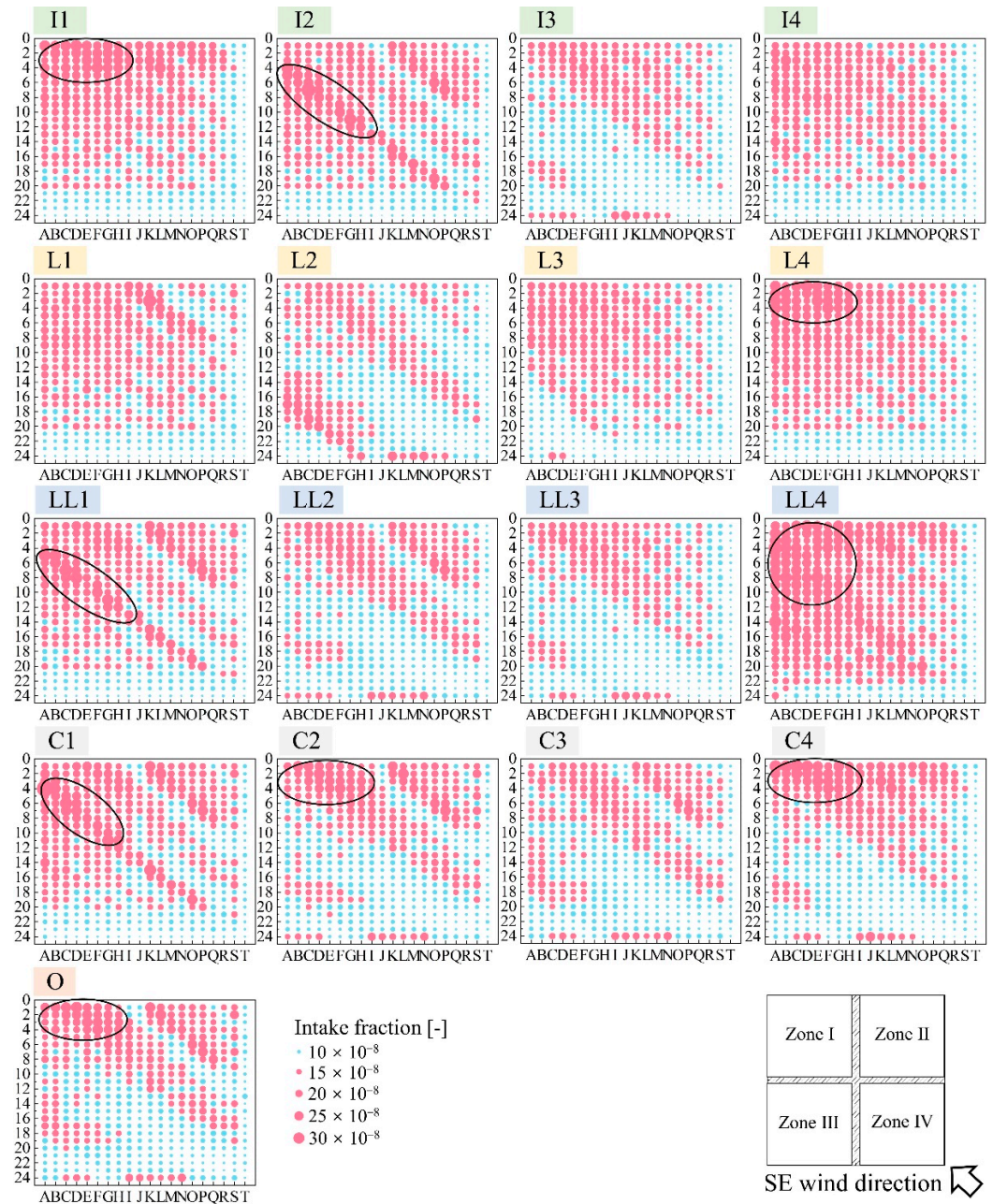


Figure 13. Analysis of the intake fraction of courtyards in the southeast wind direction. The red circles are intake fractions greater than 15×10^{-8} , and the blue circles are intake fractions less than 15×10^{-8} . 15×10^{-8} is the average value of intake fraction for all courtyards.

4.3.2. Street

The analysis of the intake fraction for the central street in the village is shown in Figure 14. For the northwest wind direction, the northern part of NS street and the western part of WE street has low IF values. In contrast, the southern part of the NS street and the eastern part of the WE street has low IF values for the southeast wind direction. In addition, morphology I1, L4, LL4, C1, C4, and O have lower IF value zones for NS streets, and morphology I1, L4, LL1, LL4, C1, C2, C4, and O have more low IF value zones for WE streets in the northwest wind direction. In general, the multi-story buildings in the northern

or western part of the village are conducive to the ventilation of the central street in the northwest wind direction. For the southeastern wind direction, the percentage of low exposure risk areas for morphology I2, I3, L2, LL1, LL2, C1, C2, C3, and O is greater than 50%. Morphology I3, L2, LL2, LL3, C2, C3, C4, and O have over 50% low exposure risk zones in the WE streets.

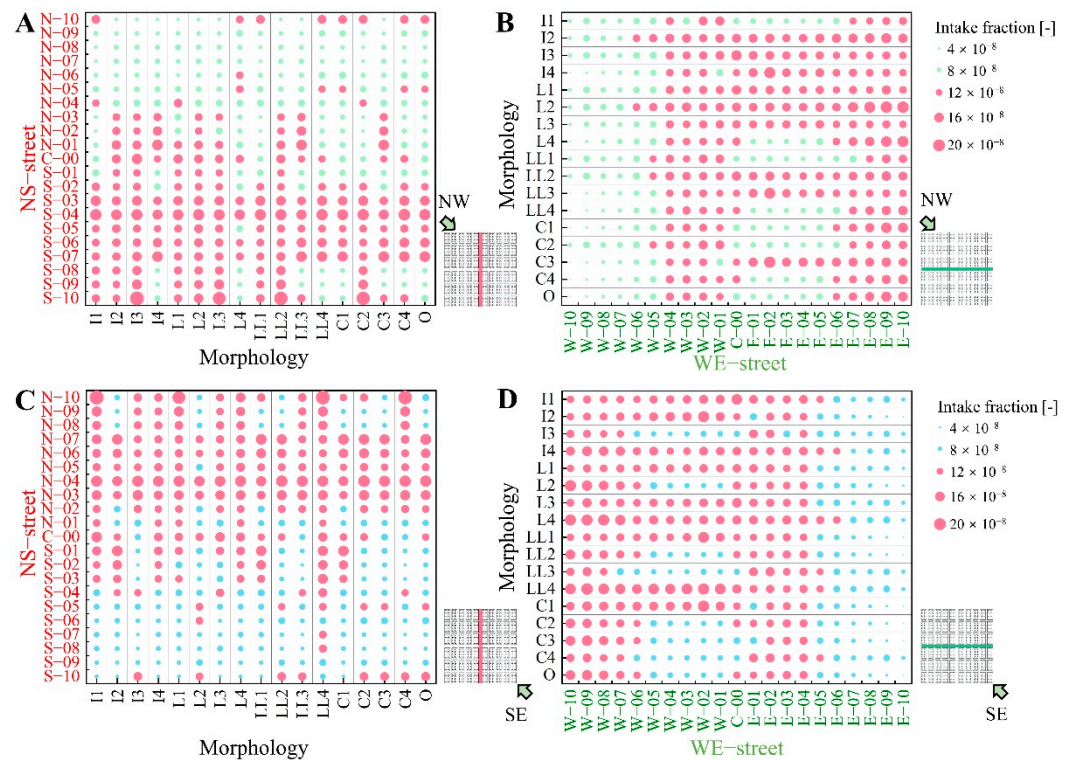


Figure 14. Intake fraction of the different zone in the central street. (A) and (B) under northwest wind direction (NW). (C) and (D) under southeast wind direction (SE). The red circles are intake fractions greater than 12×10^{-8} , and the green and blue circles are intake fractions less than 12×10^{-8} . 12×10^{-8} is the average value of intake fraction for all street zones.

4.4. Development Suggestions

In order to evaluate the overall situation of village ventilation in different village morphologies to provide village development suggestions, the average PFR values of all courtyards and streets in a particular wind direction were analyzed, as shown in Figure 15. For the courtyard space, the average PFR of morphology LL1 is the highest in the northwest wind direction, 19.9% higher than morphology I2, with the lowest average PFR. In addition, the average PFR of morphology I1, L1, L4, and C2 was at least 15% higher than that of morphology I2. In the southeast wind direction, the average PFR of the courtyards for morphology LL4 is significantly lower than the other morphologies. However, morphology I3 and LL3 had significantly higher average PFR values of the courtyards than other morphologies. For the central street space, morphology LL4 also has a very low average PFR in the southeast wind direction. The average PFR of morphology I2, L2, LL1, LL2, C1, C2, and C3 are high. For the northwest wind direction, morphology C1 has the highest average PFR, 56.1% higher than morphology L2, with the lowest average PFR. In addition, the average PFR of street space for morphology I4, L4, LL3, LL4, C3, and C4 are also high in the northwest wind direction.

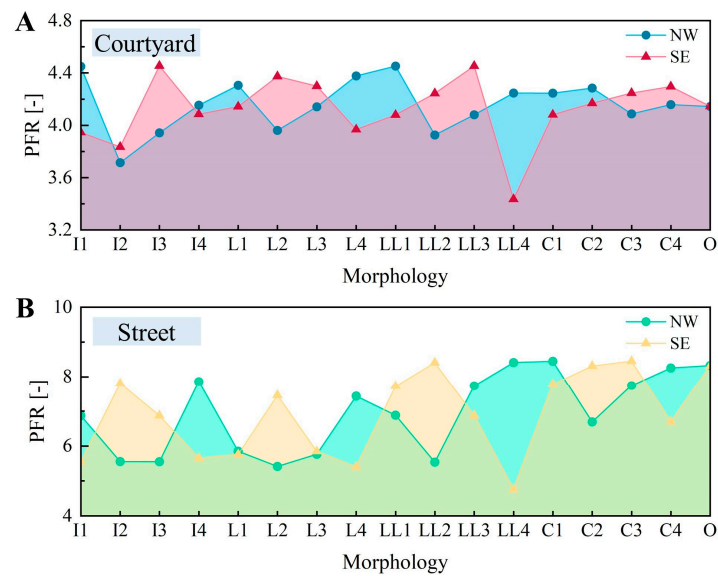


Figure 15. Average PFR for different village morphologies of the courtyard and street zones. (A) Courtyard and (B) Street.

The percentage in each case above the average intake fraction of all cases was used to evaluate how much of the zones were at high exposure risk, as shown in Figure 16. For the courtyard space, morphology LL4 had the highest percentage of high exposure risk zones in the southeast wind direction, up to 71.9%. The percentages of high exposure risk areas for morphology I3 and LL3 are low, both below 40%. For the northwest wind direction, morphology I1 and LL1 had low percentages of high exposure risk areas, both below 40%. In contrast, morphology I3 had the highest percentage of high exposure risk in the northwest wind direction, up to 60%. For the street space, the percentage of high exposure risk areas for morphology I2, I3, L2, L3, and LL2 is higher in the northwest wind direction. However, the percentages of high exposure risk areas for morphology I1, L4, LL1, LL4, C1, and O were all below 45%. In the southeast wind direction, LL4 had the highest percentage of high exposure risk at 78.6%.

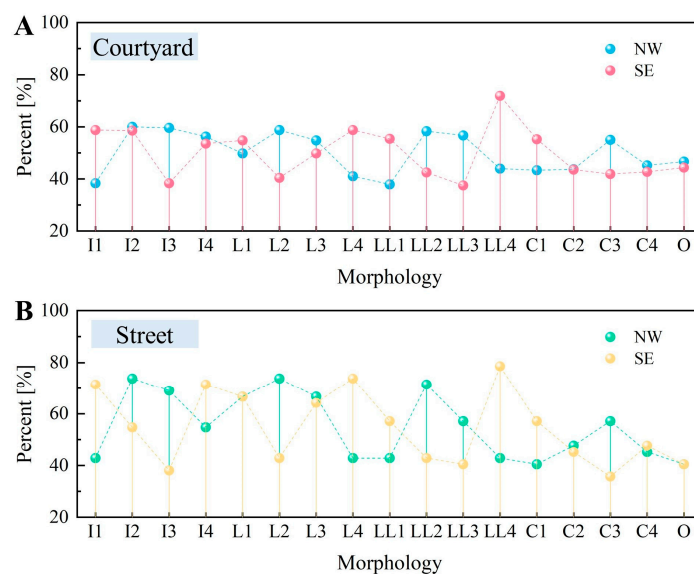


Figure 16. Percentage of intake fractions for courtyard and street zones with different morphologies greater than the average value for each wind direction. (A) Courtyard and (B) Street.

This study used star ratings to assess the optimal village morphology, as shown in Table 2. The average PFR in the top 50% obtained one star, and the percentage of intake fractions greater than all cases' average in the bottom 50% obtained one star. Morphology I2, I4, L1, and L3 are not conducive to courtyard and street ventilation in the village, and they all received only one star. However, morphology C2 and C4 both received seven stars. Therefore, these two morphologies are the best of the typical village morphology from the perspective of village ventilation and residents' health. In addition, morphology O, C1, and C3 also obtained high star numbers. Overall, morphology C is more favorable for village ventilation and residents' health, and morphology C2 and C4 are superior.

Table 2. Comprehensive assessment of village morphology.

	Morphology	I1	I2	I3	I4	L1	L2	L3	L4	LL1	LL2	LL3	LL4	C1	C2	C3	C4	O
PFR	Courtyard (NW)	*				*			*	*			*	*	*		*	
	Courtyard (SE)			*			*	*			*	*		*	*	*	*	*
	Street (NW)				*				*		*	*	*	*	*	*	*	*
	Street (SE)		*				*			*	*			*	*	*	*	*
Per_IF	Courtyard (NW)	*							*	*			*	*	*		*	*
	Courtyard (SE)			*			*				*	*		*	*	*	*	*
	Street (NW)	*							*	*			*	*	*		*	*
	Street (SE)			*			*				*	*		*	*	*	*	*
	Total star number	3	1	3	1	1	4	1	4	4	4	4	4	5	7	5	7	6

PFR is the average PFR of all courtyards or streets in one morphology case. Per_IF is the percentage of intake fractions for courtyard and street zones greater than all cases' average value for each wind direction; refer to Figure 16. PFR values in the top 50% obtain one star. Per_IF values in the bottom 50% receive one star.

5. Conclusions

Currently, research on outdoor ventilation and building morphology focus on urban areas. Rapid economic development leads to the countryside's morphology changing dramatically. However, the study of the village morphology is very scarce. This study contributed to rural morphological studies and provided suggestions for future village planning in North China. Seventeen typical village morphologies were obtained by investigating real village morphologies in Tianjin. The authors used CFD simulation results to analyze the village ventilation and the residents' health risks. Optimal countryside development morphologies were obtained through analyzing statistical data. The main study findings are as follows.

1. For the northwest wind direction, the ventilation capacity of the courtyard in the northern part of the village can be improved when there are multi-story buildings in the north or west of the village. For the southeast wind direction, when multi-story buildings exist in the south and east of the village, the ventilation capacity of the courtyard in the southern part of the village can be improved.
2. When there are multi-story buildings in the south of the village, the southern part of the village tends to form a high exposure risk area in the northwest wind direction. For the southeast wind direction, multi-story buildings in the north of the village are more likely to form a high exposure risk area in the northern part of the village.
3. Morphology C2 and C4 both obtained seven stars, which are the best of the typical village morphologies for courtyard and central street ventilation. In addition, morphology O, C1, and C3 also received high star numbers, with six, five, and five stars, respectively.
4. Morphology C is recommended for constructing multi-story residential buildings in the countryside of Tianjin. The morphologies without multi-story buildings in the west only (C2) and east only (C4) of the village are optimal.
5. For a more generalized conclusion of other North China villages with different wind directions, the windward side of surrounding multi-story buildings increases the

speed of the village's incoming winds but also blocks the airflow when located on the opposite side.

This study provided some suggestions for future village development in Tianjin. Some multi-story buildings increase the ventilation in the courtyards and central streets due to their disturbing effect on the airflow, which increases the local wind speed. In the future, the authors will simulate more realistic rural pollutant dispersion problems, such as pollutant dispersion from biomass fuel combustion, to provide more suggestions for rural construction.

Author Contributions: Conceptualization, methodology, and writing—original draft, F.X.; writing—review and editing, supervision, project administration, and funding acquisition, Z.G.; Morphological statistics, Y.X., Z.W., Y.L. and Y.H.; software, J.Z. All authors have read and agreed to the published version of the manuscript.

Funding: This research was financially supported by the opening project of the Joint International Research Laboratory of Eco-Urban Design (Tongji University), Ministry of Education (project number: 20210302).

Institutional Review Board Statement: Not applicable.

Informed Consent Statement: Not applicable.

Data Availability Statement: Not applicable.

Conflicts of Interest: The authors declare no conflict of interest.

References

1. Yim, S.H.L.; Fung, J.C.H.; Lau, A.K.H.; Kot, S.C. Air ventilation impacts of the “wall effect” resulting from the alignment of high-rise buildings. *Atmos. Environ.* **2009**, *43*, 4982–4994. [[CrossRef](#)]
2. Ramponi, R.; Blocken, B.; de Coo, L.B.; Janssen, W.D. CFD simulation of outdoor ventilation of generic urban configurations with different urban densities and equal and unequal street widths. *Build. Environ.* **2015**, *92*, 152–166. [[CrossRef](#)]
3. Tominaga, Y.; Stathopoulos, T. CFD simulation of near-field pollutant dispersion in the urban environment: A review of current modeling techniques. *Atmos. Environ.* **2013**, *79*, 716–730. [[CrossRef](#)]
4. Kastner-Klein, P.; Berkowicz, R.; Britter, R. The influence of street architecture on flow and dispersion in street canyons. *Meteorol. Atmos. Phys.* **2004**, *87*, 121–131. [[CrossRef](#)]
5. Yi, Y.; Shen, G.; Zhang, C.; Sun, H.; Zhang, Z.; Yin, S. Quantitative analysis and prediction of urban heat island intensity on urban-rural gradient: A case study of Shanghai. *Sci. Total Environ.* **2022**, *829*, 154264. [[CrossRef](#)]
6. He, B.-J.; Ding, L.; Prasad, D. Relationships among local-scale urban morphology, urban ventilation, urban heat island and outdoor thermal comfort under sea breeze influence. *Sust. Cities Soc.* **2020**, *60*, 102289. [[CrossRef](#)]
7. Zhang, Z.; Zhao, X.; Mao, R.; Xu, J.; Kim, S.-J. Predictability of the winter haze pollution in Beijing–Tianjin–Hebei region in the context of stringent emission control. *Atmos. Pollut. Res.* **2022**, *13*, 101392. [[CrossRef](#)]
8. Zhang, Y.; Zhao, B. Simulation and health risk assessment of residential particle pollution by coal combustion in China. *Build. Environ.* **2007**, *42*, 614–622. [[CrossRef](#)]
9. Shen, G.; Tao, S.; Wei, S.; Chen, Y.; Zhang, Y.; Shen, H.; Huang, Y.; Zhu, D.; Yuan, C.; Wang, H.; et al. Field measurement of emission factors of PM, EC, OC, Parent, Nitro-, and Oxy- Polycyclic Aromatic Hydrocarbons for residential briquette, coal cake, and wood in rural Shanxi, China. *Environ. Sci. Technol.* **2013**, *47*, 2998–3005. [[CrossRef](#)]
10. Cai, S.; Li, Q.; Wang, S.; Chen, J.; Ding, D.; Zhao, B.; Yang, D.; Hao, J. Pollutant emissions from residential combustion and reduction strategies estimated via a village-based emission inventory in Beijing. *Environ. Pollut.* **2018**, *238*, 230–237. [[CrossRef](#)]
11. Chen, Z.; Wang, J.-N.; Ma, G.-X.; Zhang, Y.-S. China tackles the health effects of air pollution. *Lancet* **2013**, *382*, 1959–1960. [[CrossRef](#)]
12. Zhao, K.; Zhang, Y.; Shang, J.; Schauer, J.J.; Huang, W.; Tian, J.; Yang, S.; Fang, D.; Zhang, D. Impact of Beijing's “Coal to Electricity” program on ambient PM_{2.5} and the associated reactive oxygen species (ROS). *J. Environ. Sci.* **2022**. [[CrossRef](#)]
13. Peng, Y.; Buccolieri, R.; Gao, Z.; Ding, W. Indices employed for the assessment of “urban outdoor ventilation”—A review. *Atmos. Environ.* **2020**, *223*, 117211. [[CrossRef](#)]
14. Ma, X.; Leung, T.M.; Chau, C.K.; Yung, E.H.K. Analyzing the influence of urban morphological features on pedestrian thermal comfort. *Urban CLim.* **2022**, *44*, 101192. [[CrossRef](#)]
15. Yang, J.; Yang, Y.; Sun, D.; Jin, C.; Xiao, X. Influence of urban morphological characteristics on thermal environment. *Sust. Cities Soc.* **2021**, *72*, 103045. [[CrossRef](#)]
16. Liu, Y.; Xu, Y.; Zhang, F.; Shu, W. A preliminary study on the influence of Beijing urban spatial morphology on near-surface wind speed. *Urban CLim.* **2020**, *34*, 100703. [[CrossRef](#)]

17. Peng, Y.; Gao, Z.; Buccolieri, R.; Ding, W. An investigation of the quantitative correlation between urban morphology parameters and outdoor ventilation efficiency indices. *Atmosphere* **2019**, *10*, 33. [[CrossRef](#)]
18. Peng, Y.; Gao, Z.; Buccolieri, R.; Shen, J.; Ding, W. Urban ventilation of typical residential streets and impact of building form variation. *Sust. Cities Soc.* **2021**, *67*, 102735. [[CrossRef](#)]
19. Shen, J.; Gao, Z.; Ding, W.; Yu, Y. An investigation on the effect of street morphology to ambient air quality using six real-world cases. *Atmos. Environ.* **2017**, *164*, 85–101. [[CrossRef](#)]
20. Zheng, X.; Montazeri, H.; Blocken, B. Impact of building façade geometrical details on pollutant dispersion in street canyons. *Build. Environ.* **2022**, *212*, 108746. [[CrossRef](#)]
21. Xie, X.; Huang, Z.; Wang, J.-S. Impact of building configuration on air quality in street canyon. *Atmos. Environ.* **2005**, *39*, 4519–4530. [[CrossRef](#)]
22. Huang, Y.; He, W.; Kim, C.-N. Impacts of shape and height of upstream roof on airflow and pollutant dispersion inside an urban street canyon. *Environ. Sci. Pollut. Res.* **2015**, *22*, 2117–2137. [[CrossRef](#)] [[PubMed](#)]
23. Takano, Y.; Moonen, P. On the influence of roof shape on flow and dispersion in an urban street canyon. *J. Wind Eng. Ind. Aerodyn.* **2013**, *123*, 107–120. [[CrossRef](#)]
24. Wen, C.-Y.; Juan, Y.-H.; Yang, A.-S. Enhancement of city breathability with half open spaces in ideal urban street canyons. *Build. Environ.* **2017**, *112*, 322–336. [[CrossRef](#)]
25. Chen, L.; Mak, C.M. Integrated impacts of building height and upstream building on pedestrian comfort around ideal lift-up buildings in a weak wind environment. *Build. Environ.* **2021**, *200*, 107963. [[CrossRef](#)]
26. Sha, C.; Wang, X.; Lin, Y.; Fan, Y.; Chen, X.; Hang, J. The impact of urban open space and ‘lift-up’ building design on building intake fraction and daily pollutant exposure in idealized urban models. *Sci. Total Environ.* **2018**, *633*, 1314–1328. [[CrossRef](#)] [[PubMed](#)]
27. Kubota, T.; Miura, M.; Tominaga, Y.; Mochida, A. Wind tunnel tests on the relationship between building density and pedestrian-level wind velocity: Development of guidelines for realizing acceptable wind environment in residential neighborhoods. *Build. Environ.* **2008**, *43*, 1699–1708. [[CrossRef](#)]
28. Hu, T.; Yoshie, R. Indices to evaluate ventilation efficiency in newly-built urban area at pedestrian level. *J. Wind Eng. Ind. Aerodyn.* **2013**, *112*, 39–51. [[CrossRef](#)]
29. Chang, C.-H.; Meroney, R.N. Concentration and flow distributions in urban street canyons: Wind tunnel and computational data. *J. Wind Eng. Ind. Aerodyn.* **2003**, *91*, 1141–1154. [[CrossRef](#)]
30. Ahmad, K.; Khare, M.; Chaudhry, K.K. Wind tunnel simulation studies on dispersion at urban street canyons and intersections—a review. *J. Wind Eng. Ind. Aerodyn.* **2005**, *93*, 697–717. [[CrossRef](#)]
31. Liu, C.-H.; Leung, D.Y.C.; Barth, M.C. On the prediction of air and pollutant exchange rates in street canyons of different aspect ratios using large-eddy simulation. *Atmos. Environ.* **2005**, *39*, 1567–1574. [[CrossRef](#)]
32. Liu, C.-H.; Cheng, W.C.; Leung, T.C.Y.; Leung, D.Y.C. On the mechanism of air pollutant re-entrainment in two-dimensional idealized street canyons. *Atmos. Environ.* **2011**, *45*, 4763–4769. [[CrossRef](#)]
33. Li, X.-X.; Liu, C.-H.; Leung, D.Y.C. Numerical investigation of pollutant transport characteristics inside deep urban street canyons. *Atmos. Environ.* **2009**, *43*, 2410–2418. [[CrossRef](#)]
34. Li, J.; Zheng, B.; Bedra, K.B.; Li, Z.; Chen, X. Effects of residential building height, density, and floor area ratios on indoor thermal environment in Singapore. *J. Environ. Manag.* **2022**, *313*, 114976. [[CrossRef](#)]
35. Hadavi, M.; Pasdarshahri, H. Investigating effects of urban configuration and density on urban climate and building systems energy consumption. *J. Build. Eng.* **2021**, *44*, 102710. [[CrossRef](#)]
36. Yuan, C.; Ren, C.; Ng, E. GIS-based surface roughness evaluation in the urban planning system to improve the wind environment—A study in Wuhan, China. *Urban CLim.* **2014**, *10*, 585–593. [[CrossRef](#)]
37. Wong, M.S.; Nichol, J.; Ng, E. A study of the “wall effect” caused by proliferation of high-rise buildings using GIS techniques. *Landsc. Urban Plan.* **2011**, *102*, 245–253. [[CrossRef](#)]
38. He, X.; Li, Y.; Wang, X.; Chen, L.; Yu, B.; Zhang, Y.; Miao, S. High-resolution dataset of urban canopy parameters for Beijing and its application to the integrated WRF/Urban modelling system. *J. Clean Prod.* **2019**, *208*, 373–383. [[CrossRef](#)]
39. Shen, C.; Shen, A.; Cui, Y.; Chen, X.; Liu, Y.; Fan, Q.; Chan, P.; Tian, C.; Wang, C.; Lan, J.; et al. Spatializing the roughness length of heterogeneous urban underlying surfaces to improve the WRF simulation—part 1: A review of morphological methods and model evaluation. *Atmos. Environ.* **2022**, *270*, 118874. [[CrossRef](#)]
40. Tominaga, Y.; Stathopoulos, T. CFD modeling of pollution dispersion in a street canyon: Comparison between LES and RANS. *J. Wind Eng. Ind. Aerodyn.* **2011**, *99*, 340–348. [[CrossRef](#)]
41. Wei, D.; Hu, X.; Chen, Y.; Li, B.; Chen, H. An investigation of the quantitative correlation between urban spatial morphology indicators and block wind environment. *Atmosphere* **2021**, *12*, 234. [[CrossRef](#)]
42. Liu, W.; Zhang, G.; Jiang, Y.; Wang, J. Effective range and driving factors of the urban ventilation corridor effect on urban thermal comfort at unified scale with multisource data. *Remote Sens.* **2021**, *13*, 1783. [[CrossRef](#)]
43. Ng, E.; Yuan, C.; Chen, L.; Ren, C.; Fung, J.C.H. Improving the wind environment in high-density cities by understanding urban morphology and surface roughness: A study in Hong Kong. *Landsc. Urban Plan.* **2011**, *101*, 59–74. [[CrossRef](#)] [[PubMed](#)]
44. National Bureau of Statistics. *The Seventh National Census*; National Bureau of Statistics: Beijing, China, 2021.

45. Ma, T.; Chen, T. Classification and pedestrian-level wind environment assessment among Tianjin's residential area based on numerical simulation. *Urban CLim.* **2020**, *34*, 100702. [[CrossRef](#)]
46. Richards, P.J.; Hoxey, R.P. Appropriate boundary conditions for computational wind engineering models using the k-e turbulence model. *Comput. Wind. Eng. Ind. Aerodyn.* **1993**, *46–47*, 145–153. [[CrossRef](#)]
47. Tominaga, Y.; Mochida, A.; Yoshie, R.; Kataoka, H.; Nozu, T.; Yoshikawa, M.; Shirasawa, T. AIJ guidelines for practical applications of CFD to pedestrian wind environment around buildings. *J. Wind Eng. Ind. Aerodyn.* **2008**, *96*, 1749–1761. [[CrossRef](#)]
48. Yoshie, R.; Mochida, A.; Tominaga, Y.; Kataoka, H.; Harimoto, K.; Nozu, T.; Shirasawa, T. Cooperative project for CFD prediction of pedestrian wind environment in the Architectural Institute of Japan. *J. Wind Eng. Ind. Aerodyn.* **2007**, *95*, 1551–1578. [[CrossRef](#)]
49. Chang, C.-H.; Meroney, R.N. Numerical and physical modeling of bluff body flow and dispersion in urban street canyons. *J. Wind Eng. Ind. Aerodyn.* **2001**, *89*, 1325–1334. [[CrossRef](#)]
50. Xu, F.S.; Yang, J.Z.; Zhu, X.W. A comparative study on the difference of CFD simulations based on a simplified geometry and a more refined BIM based geometry. *AIP Adv.* **2020**, *10*, 125318. [[CrossRef](#)]
51. Xu, F.S.; Gao, Z.; Zhang, J.S. Effects of roadside morphologies and moving vehicles on street canyon ventilation. *Build. Environ.* **2022**, *218*, 109138. [[CrossRef](#)]
52. Xu, F.S.; Gao, Z.; Zhang, J.S.; Hu, Y.Y.; Ding, W.W. Influence of typical street-side public building morphologies on the ventilation performance of streets and squares. *Build. Environ.* **2022**, *221*, 109331. [[CrossRef](#)]
53. Santiago, J.L.; Martilli, A.; Martin, F. CFD simulation of airflow over a regular array of cubes. Part I: Three-dimensional simulation of the flow and validation with wind-tunnel measurements. *Bound.-Layer Meteor.* **2007**, *122*, 609–634. [[CrossRef](#)]
54. Hang, J.; Li, Y. Age of air and air exchange efficiency in high-rise urban areas and its link to pollutant dilution. *Atmos. Environ.* **2011**, *45*, 5572–5585. [[CrossRef](#)]
55. He, L.J.; Hang, J.; Wang, X.M.; Lin, B.R.; Li, X.H.; Lan, G.D. Numerical investigations of flow and passive pollutant exposure in high-rise deep street canyons with various street aspect ratios and viaduct settings. *Sci. Total Environ.* **2017**, *584*, 189–206. [[CrossRef](#)]
56. Du, X.; Wu, Y.; Fu, L.X.; Wang, S.X.; Zhang, S.J.; Hao, J.M. Intake fraction of PM_{2.5} and NO_x from vehicle emissions in Beijing based on personal exposure data. *Atmos. Environ.* **2012**, *57*, 233–243. [[CrossRef](#)]